CrossMark

Preparation of High Surface Area Oxidized Activated Carbon from Peanut Shell and Application for the Removal of Organic Pollutants and Heavy Metal Ions

Jianyi Liu · Yan Liu · Jianbo Peng · Zhanchao Liu · Yinhua Jiang · Minjia Meng · Wenli Zhang · Liang Ni

Abstract A peanut shell-derived oxidized activated carbon (OAC) with high surface area was prepared by zinc chloride ($ZnCl_2$) chemical activation and subsequent nitric acid oxidation. OAC was characterized by scanning electron microscope (SEM), Fourier transform infrared spectroscopy (FT-IR), and N_2 adsorption-desorption. The results showed that OAC had the surface area of 1807 m^2 g^{-1}, with the total pore volume of 0.725 cm^3 g^{-1} and average pore diameter of 3.8 nm. More importantly, when OAC acted as an adsorbent, it exhibited high efficiency to remove basic blue 41 (BB-41), congo red (CR), phenol, Cr(VI), and Pb(II) from aqueous solution due to its universality in adsorption. Batch adsorption experiments were carried out to study the effect of various parameters such as pH, initial concentration, temperature, and contact time. Also, the isotherms, kinetic models, and thermodynamics of adsorption process were investigated. The equilibrium data for CR and Pb(II) were fitted to Langmuir isotherm model, while Freundlich model was suitable for the equilibrium isotherm of BB-41, phenol, and Cr(VI), respectively. As the result indicated, peanut shell was a suitable raw material to synthesize OAC which could be employed as an efficient and universal adsorbent for removing organic pollutants and heavy metal ions from wastewater.

1 Introduction

In recent years, the incomplete removal of toxic pollutants in wastewater has led to a series of environmental problems in many industries. Especially, the wastewater contains concentrated organic pollutants, and heavy metal ions present a significant threat to human health because of the toxicity, accumulation, and persistence in nature. Many different approaches, including chemical precipitation, membrane separation, ion exchange, and adsorption strategies have been used for the treatment of industrial effluents (Bonvin et al. 2015). Among these methods, the adsorption technique is regarded as the most promising one for removing different types of pollutions. A large number of materials have been used as adsorbents for the removal of toxic pollutants from aqueous solutions, such as zeolites (Piccini et al. 2015), graphene oxide, carbon nanotubes (Li et al. 2013), imprinted polymer (Liu et al. 2014; Liu et al. 2016), and so on. In the past years, in the quest for easily accessible, low-price, and effective adsorbents, various natural materials and by-products like rice husk (Kumar

J. Liu (✉) · Y. Liu · J. Peng · Y. Jiang · M. Meng · W. Zhang · L. Ni
School of Chemistry and Chemical Engineering, Jiangsu University, Zhenjiang 212013, China
e-mail: leojoyi@163.com

Z. Liu
School of Materials Science and Engineering, Jiangsu University of Science and Technology, Zhenjiang 212003, China

and Kumar 2015), pistachio hull (Moussavi and Khosravi 2011), soybean straw (Bo et al. 2008), and coniferous pinus bark (Ahmad 2009) have attracted immense interest. However, due to the particularities and complexity of wastewater which contain different molecular size and charged toxic pollutants, these traditional materials showed limited potential to adsorb pollutants, such as low adsorption capacity, adsorption single pollutant, and so on. Therefore, it is urgent to develop an efficient, low cost, and universal adsorption material.

Activated carbon (AC) has been widely used as an adsorbent in the separation and purification processes for wastewater treatment due to its high surface area, large porosity, well-developed internal pore structure, and a wide spectrum of functional groups present on the surface. AC can be prepared from a variety of carbonaceous precursors. In order to reduce the cost of AC preparation, agricultural by-products are gaining great importance as precursors for AC production. Many agricultural by-products, such as Kenaf core fiber (Shamsuddin et al. 2016), waste cotton fibers (Ekrami et al. 2014), Buriti shells (Pezoti et al. 2014), bamboo (Lo et al. 2012), coffee residue (Boonamnuayvitaya et al. 2005), walnut shells (Yu et al. 2014), etc. have been successfully converted into low-cost AC. Peanut shell is a good amount of agro-waste produced in planting industry. It is not used for any industrial purposes. There would be an environmental damage if not dealt immediately. However, peanut shell is of a low ash content, low apparent density, and high degree of porosity which is assured as a promising precursors to synthesis AC. Thus, the conversion processing of peanut shell for AC could ease the environmental pollution of peanut shell and reduce the cost of AC.

The preparation method of AC includes chemical and physical activation. Generally, the physical activation method involves the carbonization of a carbonaceous precursor and the subsequent activation at high temperature (800–1000 °C) in a carbon dioxide or steam atmosphere. The chemical activation is a single-step activation schemes with the presence of chemical agent (e.g., $ZnCl_2$, KOH, and H_3PO_4) (Muniandy et al. 2014). Comparing to physical activation, the chemical activation process takes place at a lower temperature (500–800 °C) and higher carbon yields are produced. Among these chemical agents, AC with a larger amount of micro- and mesoporosity is prepared by $ZnCl_2$ activation compared to others because the mechanism for

$ZnCl_2$ activation is somewhat different (Guo and Lua 2003; Ruiz-Fernández et al. 2011; Serkan Timur et al. 2013). $ZnCl_2$ dissolves the cellulose inside the peanut shell, followed by catalytic dehydration at high temperatures. It results in charring and aromatization of the carbon skeleton and creation of the pore structure. As a result, $ZnCl_2$ could be the best activating agent to prepare activated carbon with high surface area.

Adsorption processes are influenced by a number of factors, which mainly consist the physical-chemical characteristics of the adsorbent. The adsorption properties of AC can be significantly influenced by surface functional groups including carbonyl, carboxyl, lactones, quinones, and so on. The nature and contents of surface functional groups on AC may be modified by suitable thermal or post-chemical treatment to improve its adsorption performance for contaminant removal. Many methods have been reported to modify the surface of AC which enable higher uptake of specific pollutants, such as base treatment (Saleh and Danmaliki 2016), microwave treatment (Hesas et al. 2013), ozone treatment (Jaramillo et al. 2010), etc. However, some of these methods need expensive equipments, complicated operation, and high energy consumption or have a decrease in hydrophilicity. Compared with these approaches, acid treatment has excellent performance, including cost effectiveness, ease of operation, and energy saving. Acid treatment is generally employed to oxidize the surface of AC and obtain oxidized activated carbon (OAC) as it increases the acidic property, removes the mineral elements, and improves the hydrophilic nature of surface. The negatively charged acid groups of OAC have a tendency to connect and adsorb organic pollutants and metal ions (Bhatnagar et al. 2013). The nitric acid and sulfuric acid are the most widely studied for improving the surface acidic functional groups (i.e., carboxyl). Chen et al. (2015)) prepared cotton-derived porous carbon and oxidized it with nitric acid, the adsorption capacities significantly increased after nitric acid modification.

In this work, a high surface area OAC was first synthesized using peanut shell as raw material by $ZnCl_2$ activation at 500 °C and further oxidized with concentrated nitric acid. Subsequently, it was applied as an adsorbent for the removal of organic pollutants and heavy metal ions from aqueous solution and exhibited universality and high capacities in adsorption. Basic blue 41 (BB-41), congo red (CR), phenol, Cr(VI), and Pb(II) were used as organic pollutants and heavy metal ion

model, respectively. The major adsorption influencing factors contain pH; initial concentration and contact time were investigated in batch adsorption experiment.

2 Experimental

2.1 Chemicals and Materials

The peanut shell was provided from a local market in Zhenjiang, China. The sample was washed thoroughly with distilled water to remove clay and then dried in air at 105 °C in an oven for 24 h and crushed with geometrical mean size ranging from 40 to 60 meshes (0.42–0.25 mm). All AR-grade chemicals were used. Basic blue 41 (BB-41, molecular formula: $C_{20}H_{26}N_4O_6S_2$), congo red (CR molecular formula: $C_{32}H_{22}N_6Na_2O_6S_2$), and phenol (molecular formula: C_6H_6O) were used as organic pollutant model which were purchased from Sigma-Aldrich (Shanghai, China). For the metal ion adsorption, Pb(II) and Cr(VI) were applied as the metal ion pollutant model and come from $Pb(NO_3)_2$ and $K_2Cr_2O_7$, respectively. Other chemicals including $ZnCl_2$, HCl, $Pb(NO_3)_2$, NaOH, KOH, H_3PO_4, $K_2Cr_2O_7$, $NH_3 \cdot H_2O$, and HNO_3 were purchased from Sinopharm Chemical Reagent Company (Shanghai, China). For all the experiments, double distilled water was used.

2.2 Instruments and Measurements

Fourier transmission infrared spectra (FT-IR) analysis was performed on a Nicolet NEXUS-470 FT-IR spectrometer (USA), using 24 scans per spectrum in the region of 4000–400 cm^{-1}. Scanning electron microscopy (SEM) was recorded by using the JEOL JSM-6480 microscope at an accelerating voltage of 25 kV. The specific surface area, total pore volume, and pore size distribution analyses were measured at − 196 °C using a NOVA 2000 surface area and pore size analyzer (Quntachrome, USA); the specific surface areas (SBET) were calculated by the Brunauer–Emmett–Teller (BET) method. The Barrett–Joyner–Halenda (BJH) model was used to derive the pore size distributions. The concentrations of organic samples in the supernatant solutions were analyzed by a UV-Vis spectrophotometer (JASCO V570, Japan). The concentrations of metal ions were determined by VISTA-MAX Inductive Coupled Plasma-Atomic Emission Spectrometer (ICP-AES, Varian, USA). The zeta potential of OAC in different pH solutions was analyzed by a zeta meter (Zeta-Meter, PG314, USA).

2.3 Preparation of Activated Carbon

Five grams of dried peanut shell powders were impregnated with 100 mL of 10% $ZnCl_2$ solution at 85 °C for 2 h under stirring. After impregnation, the sample was dried 100 °C for 12 h. The obtained material was placed in a tubular furnace, followed by heating to 500 °C at an increasing rate of 3 °C min^{-1} and maintaining at this temperature for 1 h under N_2 flow protection. After cooling to room temperature, the obtained sample was thoroughly washed with distilled water and dried for 12 h at 105 °C, and then, the activated sample was ground to obtain AC.

2.4 Preparation of Oxidized Activated Carbon

Three different types of OAC were prepared successfully. The obtained AC was dispersed in 10 mol L^{-1} HNO_3, H_3PO_4, and KOH, respectively. Then, those mixture solutions were refluxed and agitated at 100 °C for 24 h. After draining the acidic solution, those samples were washed with distilled water to remove residual chemicals until the pH of the wash water was neutral, and then dried in an oven at 105 °C for 12 h, the obtained samples were labeled OAC, OAC-P, and OAC-K, respectively.

The scheme of processes is shown in Scheme 1. It was reported that $ZnCl_2$ acted as a dehydration agent to promote the cross-linking and activate of various materials (Ahmadpour and Do 1996; Yue et al. 2002). It caused hydrogen and oxygen atoms in the source materials to be stripped away. Impregnation with $ZnCl_2$, first results in degradation of the cellulosic material and on carbonization on produces dehydration that results in charring and aromatization of the carbon skeleton and creation of the pore structure (Ahmadpour and Do 1996). After removing $ZnCl_2$ with washing, the large specific surface area and porosity of AC was obtained. The acidic treatment of AC occurred in HNO_3 solution at 100 °C for 24 h and the product was rinsed with distilled water until the pH reaches neutral and then dried to obtain OAC. OAC possess more diverse oxygen functional groups on the surface after nitric acid oxidation, including –OH and –COOH. Moreover, there are some adsorption interaction including hydrogen
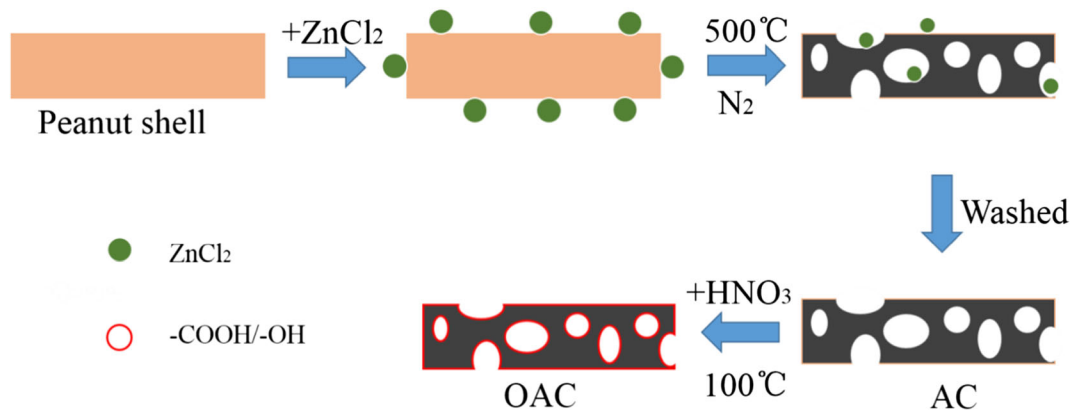
Scheme 1 The synthesis route of OAC

bonding and electrostatic attraction between these functional groups (–OH/–COOH) and adsorbate when OAC was used as an adsorbent. The method introduced oxygen functional groups in OAC without changing its textural parameters significantly (Bhatnagar et al. 2013).

2.5 Static Adsorption Studies

The equilibrium and kinetic adsorption process were investigated in static batch experiments. Static adsorption experiments were performed at controlled pH and ambient temperature. In a typical adsorption process, OAC (10 mg) was added into a glass colorimetric tube containing 20 mL of organic pollutant/metal ion aqueous solution. The pH of organic pollutant solution was adjusted by 0.1 mol L^{-1} HCl or 0.1 mol L^{-1} NaOH solution. For metal ions, 0.1 mol L^{-1} HCl or 0.1 mol L^{-1} NH$_3$·H$_2$O solution was used. All pH measurements were carried out using a pH meter (Model pHS-3C, shanghai, China). The mixture was then shaken vigorously for 10 min and the adsorption time was maintained for 12 h. After the adsorption for 12 h, the amount of organic pollutants/metal ions per unit weight of adsorbent, q_e (mg g^{-1}) at equilibrium and q_t (mg g^{-1}) at time t (min) was determined by the mass balanced equation:

$$q_e = \frac{(C_0 - C_e)V}{M} \tag{1}$$

$$q_t = \frac{(C_0 - C_t)V}{M} \tag{2}$$

where C_0, C_e, and C_t are the concentrations of adsorbates at initial, equilibrium, and time t (mg L^{-1}),

respectively. M is the mass of adsorbent (g). V is the volume of adsorption solution (L).

2.6 Adsorption Isotherm and Kinetic Models

A number of isotherms and models have been developed to explore the relationship between the parameters of the adsorption process and investigate the controlling mechanism of adsorption processes such as mass transfer and chemical reaction. Two isotherm models (Langmuir and Freundlich) and two kinetic models (pseudo-first-order and pseudo-second-order) were used to fit the experimental data. The equations and parameters of the isotherm and kinetic models are listed as follows.

Langmuir isotherm

$$q_e = \frac{q_m K_L C_e}{1 + K_L C_e} \tag{3}$$

$$R_L = \frac{1}{1 + K_L C_0} \tag{4}$$

Freundlich isotherm

$$lnq_e = lnK_F + \frac{1}{n_F} lnC_e \tag{5}$$

Pseudo-first-order kinetic

$$q_t = q_e\left(1 - e^{-k_1 t}\right) \tag{6}$$

Pseudo-second-order kinetic

$$q_t = \frac{k_2 q_e^2 t}{1 + k_2 q_e t} \tag{7}$$

C_0 and C_e are the concentration of adsorbate at initial and equilibrium (mg L^{-1}), respectively; q_e is the amount

of adsorbate adsorbed per unit of the adsorbent at equilibrium (mg g^{-1}); q_m is the maximum adsorption capacity (mg g^{-1}); K_L is the Langmuir constant; K_F and n_F stand for the Freundlich constants; R_L is the separation factor; k_1 and k_2 are the pseudo-first-order and pseudo-second-order adsorption rate constant, respectively; t is the contact time (min); q_t is the adsorption capacity at any time (mg g^{-1}).

2.7 Desorption Experiments

After adsorption experiments, some methods have been employed to elute the organic pollutants and heavy metal ions. A mixture of water and methanol in volume proportion 1:1 was used to desorb BB-41. The adsorbent that was used for the adsorption of CR was washed gently with 0.1 M HCl solution, and CH_3COOH solution (50% *v/v*) to remove CR. Desorption studies of phenol were conducted using 0.1 M NaOH solution. For Cr(VI), the desorption conditions were a stripping solution of 20% H_2SO_4 and a contacting time of 4 h. Pb(II)-laden OAC was separated out by filtration and the filtrate was discarded. Desorption studies were carried out using OAC agitated with 0.1 M HCl solution. Subsequently, the OAC was separated by centrifugation, washed by distilled water several times, until neutralization, and then reused in the next cycle of adsorption experiment.

3 Results and Discussion

3.1 Characterization of the Oxidized Activated Carbon

3.1.1 Characterization of FT-IR

FT-IR spectra of AC and OAC are obtained to identify the oxidation mechanism. As shown in Fig. 1, compared with OAC, AC shows no obvious adsorption peaks. The FT-IR spectrum of the OAC confirmed the presence of functional groups, including –OH (3432 cm^{-1}) and –COOH (1721 cm^{-1}). It means that OAC possess more diverse oxygen functional groups on the surface after nitric acid oxidation. These functional groups are hydrophilic which improve the dispersible of OAC in water (Shen et al. 2008). When it acts as an adsorbent, there are some adsorption interaction including hydrogen bonding and electrostatic
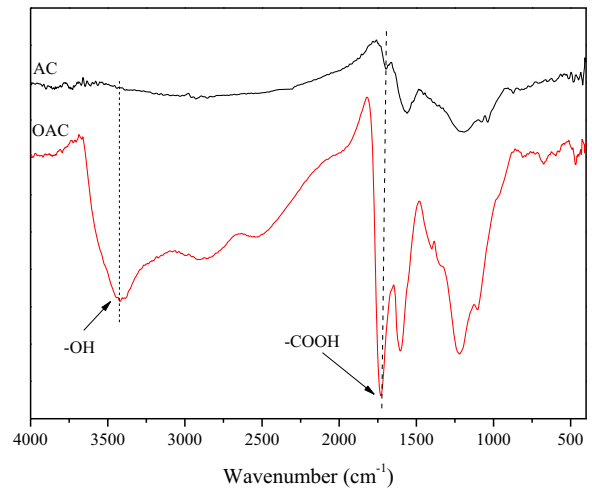

Fig. 1 FT-IR spectra of activated carbon and oxidized activated carbon

attraction between these functional groups (–OH/–COOH) and adsorbate, which imply toward wider adsorbate and larger adsorption capacity.

3.1.2 Characterization of SEM

The morphologies of the carbonized peanut shell and OAC are shown in the SEM images (Fig. 2). Figure 2a shows that the carbonized peanut shell possesses a discontinuous bulk structure. The image of OAC (Fig. 2b) shows that a discontinuous, rough, and irregular surface originates from a large number of cavities on the surface, caused by the dehydrating action of activating agent. The obviously rough surfaces and a large number of cavities denote a large specific surface area for adsorption. As shown in Fig. 2c, the porosity of the oxidized activated carbons arises from randomly distributed micro-pores. The porosity of the oxidized activated carbons is probed by N_2 adsorption-desorption analysis."

3.1.3 N_2 Adsorption-Desorption Analysis

Nitrogen adsorption-desorption isotherm and pore size distribution plot are displayed in Fig. 3. It is clear that the shape of the isotherm refers to the type IV isotherm according to International Union of Pure and Applied Chemistry (IUPAC) classification in Fig. 3a. Besides, the isotherm also demonstrates a marked hysteresis, demonstrating the existence of a large number of mesoporous in OAC (Njoku et al. 2014). As shown in
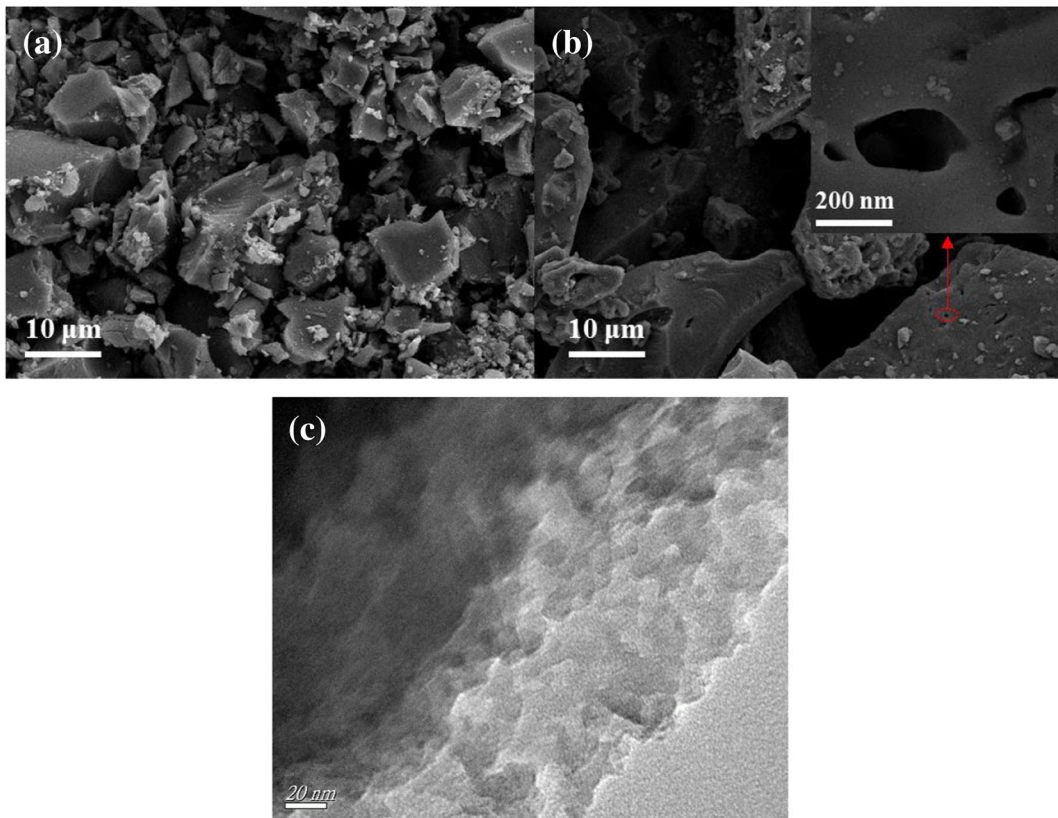
Fig. 2 SEM image of peanut shell after carbonization (**a**), oxidized activated carbon (**b**), and partial enlargement of the pores (inset) and TEM image of oxidized activated carbon (**c**)

Table 1, the specific surface area (S_{BET}) of OAC, OAC-P, and OAC-K is calculated to be 1807, 855, and 1081 m^2 g^{-1}, respectively. It is implied that greater micro- and mesoporosity developments are obtained

with ZnCl$_2$ activation compared to other chemical activating agents. Compared with the previous work (Gomez-Serrano et al. 2005), the largest surface area of OAC and other ACs from agricultural by-products

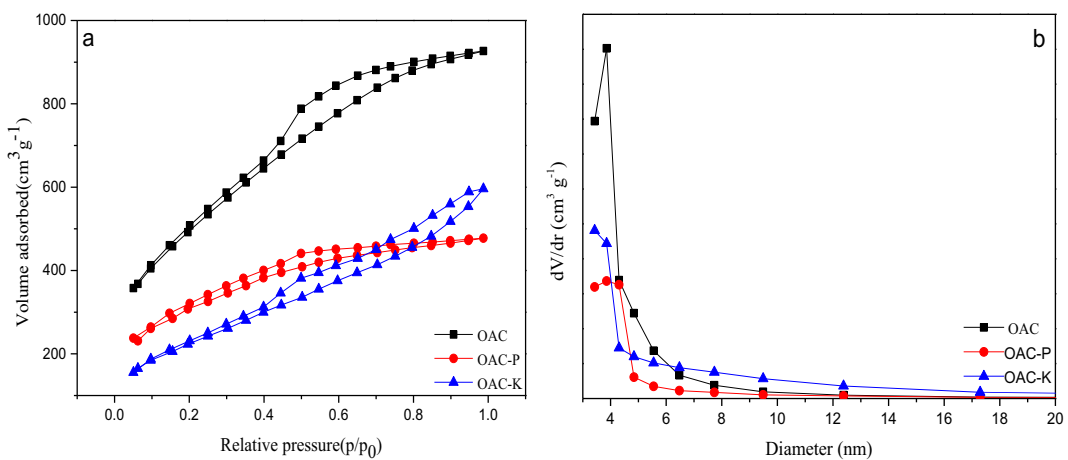**Fig. 3** Nitrogen adsorption-desorption isotherm (**a**) and Barrett-Joyner-Halenda (BJH) adsorption pore-size distribution plot (**b**) of oxidized activated carbon, oxidized activated carbon-H$_3$PO$_4$, and oxidized activated carbon-KOH, respectively

Table 1 Surface areas and pore volumes of oxidized activated carbon, oxidized activated carbon-H$_3$PO$_4$, and oxidized activated carbon-KOH

Material	S_{BET} (m^2 g^{-1})	V_T (cm^3 g^{-1})	D_P (nm)
OAC	1807	0.725	3.8
OAC-P	855	0.654	3.4
OAC-K	1081	0.270	3.4

activated by H$_3$PO$_4$ and KOH are 1636 and 747, respectively. It shows that the high surface area activated carbon can be prepared from the peanut shell with ZnCl$_2$ activation. A comparison of the surface area of different activated carbons and other adsorbent is listed in Table 2; the results show that the high surface area activated carbon can be prepared from the peanut shell with ZnCl$_2$ activation.

3.2 Organic Pollutants and Heavy Metal Ion Adsorption

3.2.1 Zeta Potential Measurements

Figure 4 shows the zeta potential versus pH plots for OAC. An important parameter used to characterize the electro-kinetic behavior of a solid-liquid interface is the point of zero zeta potential. The pH value at this point is often called the isoelectric point (pI) of the interface. As shown in the Fig. 4, when pH value is lower than 4, these groups (–COOH/–OH) on the surface of OAC start to become protonated, and at higher pH, these
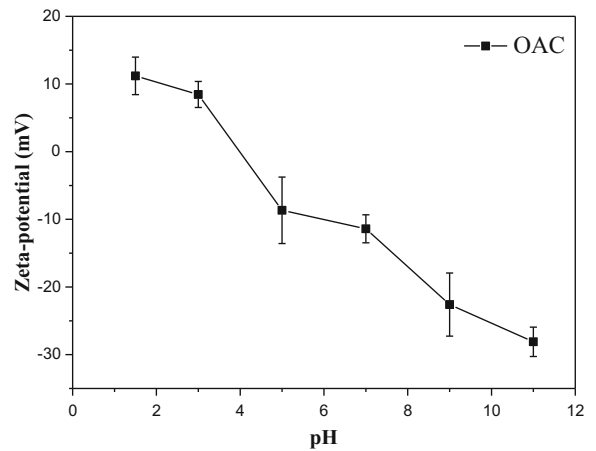
Fig. 4 Effect of pH on the zeta potential of sample OAC

groups (–COOH/–OH) become anionic (–COO$^-$/–O$^-$) due to dissociation. The pI of OAC is close to 4; it indicates that OAC surface is positively charged at lower pH and negatively charged at higher pH value. The further the pH deviates from the isoelectric point, the larger the absolute value of zeta potential becomes.

3.2.2 Effect of pH

The pH of solution plays an important factor in adsorption. Figure 5 shows that the optimum pH values of adsorption for each pollutant. Generally, solution pH affects the surface charge of adsorbent and degree of ionization of the adsorbate. For the OAC, the ionic state of the carboxyl and hydroxyl function groups on the surface is important for the adsorption process.

Table 2 Comparison of the surface area of the different activated carbons and other adsorbent

| Adsorbent	BET surface area	Reference
Fe3O4-COOH@(PAH/GO-COOH)	42.27	(Guo et al. 2017)
EDTA-AC	741	(Babu et al. 2018)
SBA-15/PAMAM	743.45	(Mirzaie et al. 2017)
Modified activated carbon (MAC)	683	(Van et al. 2018)
Activated Carbon Fiber	1156	(Berber-Mendoza et al. 2018)
Kenaf core fiber activated carbon	299.02	(Shamsuddin et al. 2016)
Cotton fibers activated carbon	694	(Ekrami et al. 2014)
Buriti shell activated carbon	843	(Pezoti et al. 2014)
Ginkgo leaves activated carbon	696.58	(Wang and Chen 2015)
Banana bunch activated carbon	981	(Salman 2014)
peanut shell activated carbon	1807	This work
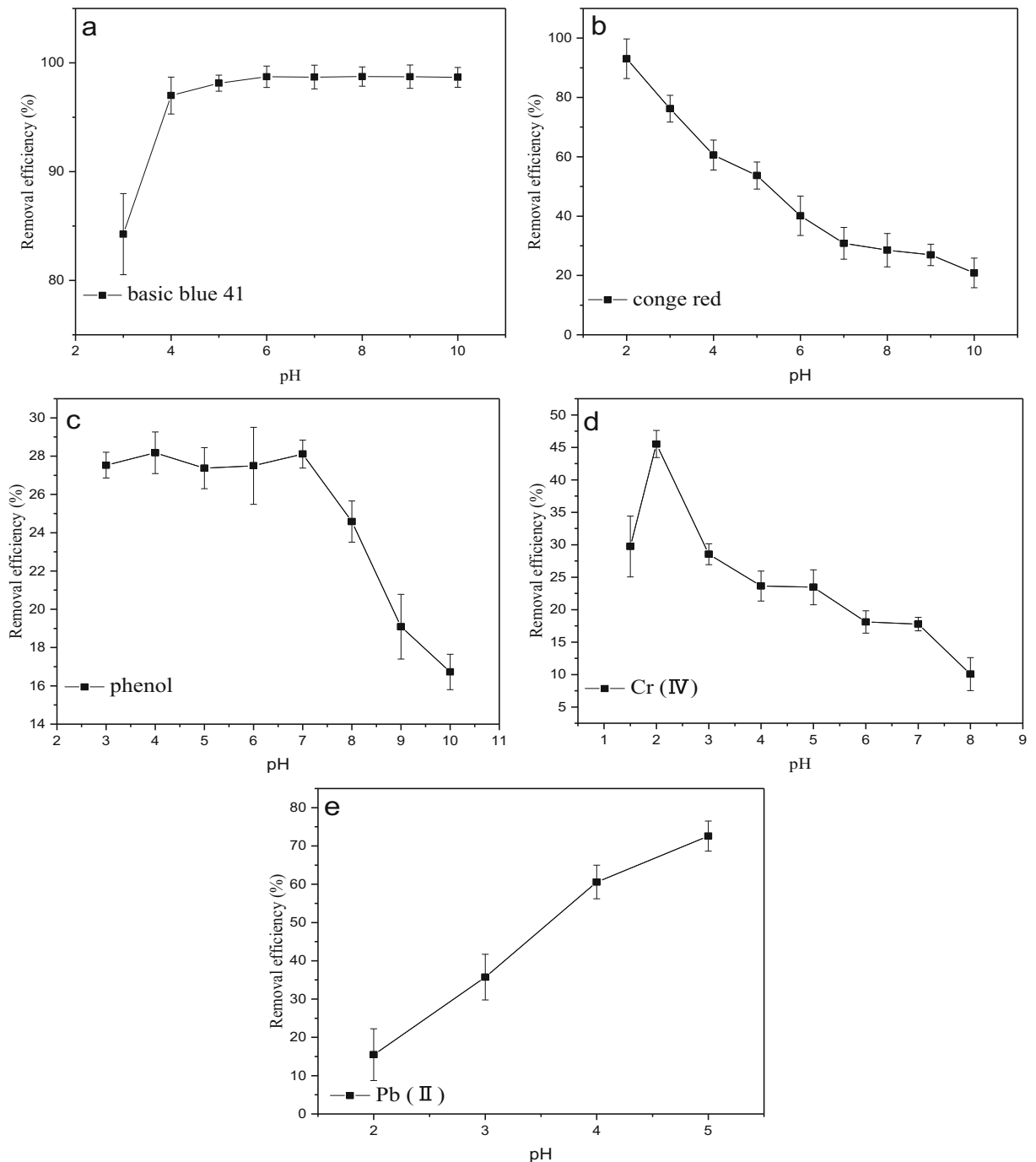
Fig. 5 The pH influences of the static adsorption about basic blue 41 (**a**), congo red (**b**), phenol (**c**), Cr(VI) (**d**), and Pb(II) (**e**) (basic blue 41, congo red, phenol: 100.0 mg L^{-1}; Cr(VI), Pb(II): 50.0 mg L^{-1})

OAC exhibits the highest removal rate of 98.8% toward BB-41. BB-41 is a cationic dye which belongs to the positively charged pollutants in solution. It can be seen that quantitative removal of BB-41 taken place at pH ranging from 3.0 to 10.0 in Fig. 5a, the removal rate

increases with the increase of pH values from 3.0 to 5.0. Further, there is no any significant change with the pH increasing. Lower adsorption of BB-41 at acidic pH is probably due to the presence of H$^+$ competing with the cationic groups on BB-41 for adsorption sites. When the

pH value increases, the surface of the activated carbon becomes negatively. Thus, the adsorption capacity of the BB-41 reaches maximum at pH 7.0.

The pH effect (2.0–10.0) on CR adsorption onto OAC was investigated, and results (Fig. 5b) confirmed that maximum CR adsorption was achieved at pH 2.0. At higher pH, these groups (–COOH/–OH) become anionic (–COO$^-$/–O$^-$) and not suitable for the adsorption of negatively charged CR. At acidic pH, CR has a property to aggregate in aqueous and organic solutions. The CR is less soluble and more readily adsorbed due to the restriction of protonation of the functional groups from CR at low pH.

For phenol, the initial solution pH values range from 3.0 to 10.0. Figure 5c shows that the phenol removal rate is unaffected when the initial pH changed from 3.0 to 7.0. The adsorption decrease at high pH values due to electrostatic repulsions between the negative surface charge and the phenolate-phenolate anions in solution. While at acidic pH, non-dissociated phenol molecules can easily be adsorbed by the partially protonated chemical groups of OAC surface due to the dispersion interaction. The dispersion force arises from the fluctuating charge distribution-instantaneous dipoles between phenol molecules and OAC.

Chromium is present in the wastewater as Cr(VI) in the form of oxyanion, such as chromates (CrO$_4^{2-}$), dichromates (Cr$_2$O$_7^{2-}$), and bichromates (HCrO$_4^-$). The pH of the solution determines the different ionic forms of the Cr(VI). Change of the adsorption capacity of Cr(VI) on OAC with pH is shown in Fig. 5d; it is observed that the adsorption capacity increases with the increase of pH and then decreases. The acidic pH leads to an increase in H$^+$ ions on the carbon surface; this results in significantly strong electrostatic attraction between the positively charged OAC surface and the negatively charged species of Cr(VI). However, the Cr(VI) presents predominantly as CrO$_4^{2-}$ and HCrO$_4^-$ at strong acidic condition. Thus, the maximum adsorption occurred at pH 2.0 and might be presented as wastewater at about pH 8.5.

It is generally recognized that the solution pH greatly influences the adsorption of heavy metals from aqueous solution onto adsorbents. To optimize the pH for maximum removal efficiency and to avoid the precipitation of Pb(II), a sorption experiment was conducted in the initial pH range from 2 to 5, as shown in Fig. 5e; it is apparent that the equilibrium adsorption amount of Pb(II) on OAC increase with increasing pH. At

pH 2.0, the competition of H$^+$ and Pb(II) ions for the same adsorption active sites. The density of negative charge on OAC increases rapidly with increasing of pH. However, Pb(II) is not stable at strong alkaline condition (Sekar et al. 2004). Therefore, the optimal operational pH is 5.0 for Pb(II). As a result, the value at pH 7.0, 2.0, 3.0, 2.0, and 5.0 was selected for BB-41, CR, phenol, Cr(VI), and Pb(II), respectively. All the following experiments were carried out at the optimum pH value.

3.2.3 Adsorption Isotherms

As shown in Fig. 6a, the adsorption capacity of BB-41 onto OAC increases sharply with the initial concentration increasing. This may be due to the fact that high initial concentration promotes the driving force to overcome the mass transfer resistance between the solid and liquid interfaces. However, when adsorption process reaches the saturated state, all the sites on the adsorbent have reached the dynamic balance. Desorption occurs simultaneously with adsorption, and the adsorption rate equals the desorption rate, so that the apparent adsorption rate is zero, and the adsorbent reaches the maximum adsorption capacity. BB-41 molecules cannot be adsorbed onto OAC even if it continue to increase the initial concentration. The adsorption of BB-41 onto OAC at different temperature shows an increase tendency in the adsorption capacity when the temperature increases. Generally, the temperature has three main effects on the adsorption processes of the porous adsorbents. Firstly, it can affect the diffusion rate of the adsorbed substance within the pores as a result of decreasing solution viscosity. Secondly, it also can affect the number of the sorption sites generated because of breaking of some internal bonds near the edge of active surface sites of sorbent, which benefits for improving the adsorption capacity of the adsorbents. Thirdly, the sorption was endothermic in nature, and a better adsorption performance can be obtained at a higher temperature. Furthermore, the same phenomenon was observed on other four adsorbates (CR, phenol, Cr(VI), and Pb(II)). Thus, increasing initial concentration and temperature can increase the driving force between the solid and the liquid interfaces, the diffusion rate of adsorbate, and the number of the adsorption sites, respectively, which enhance the adsorption ability of OAC.
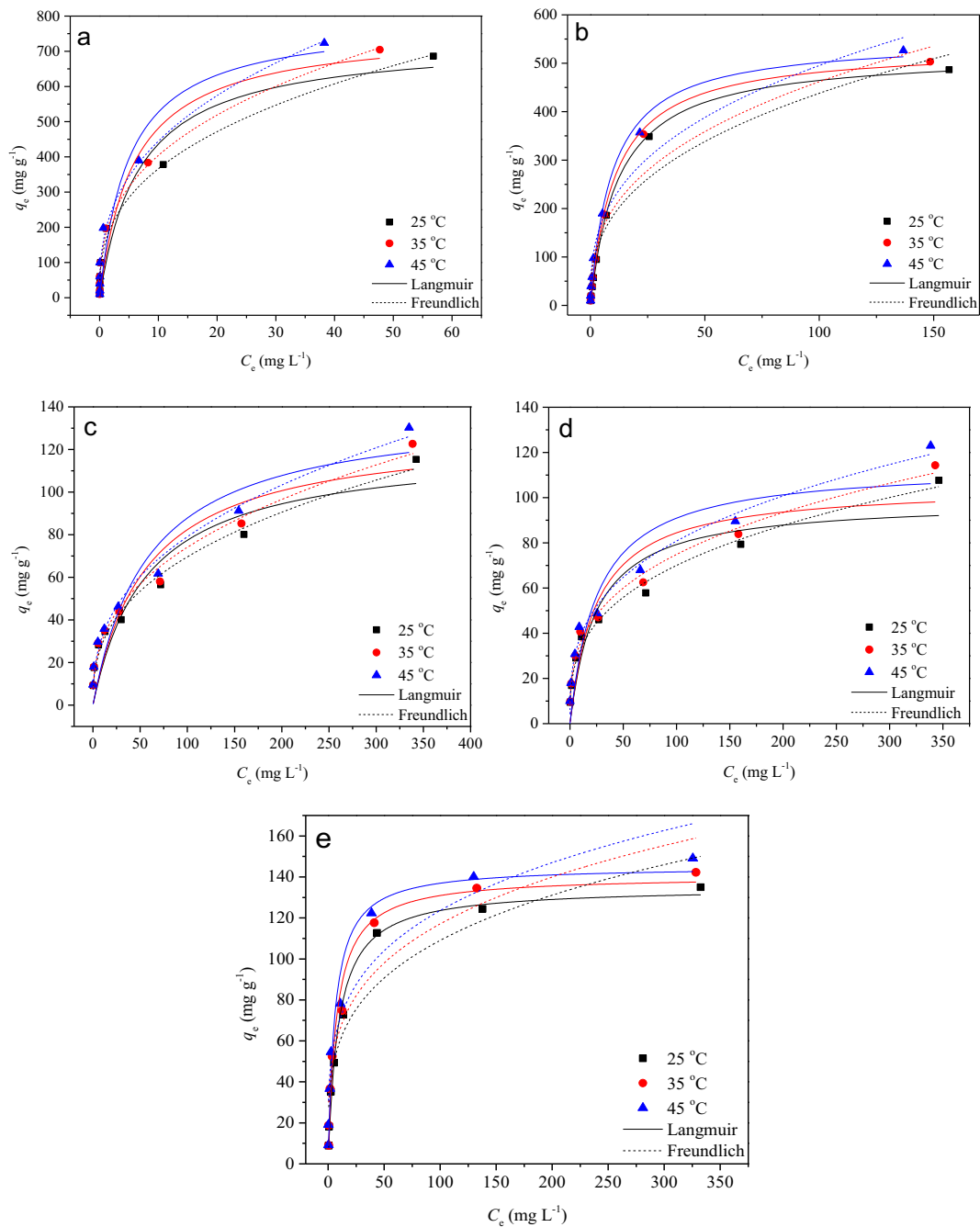
Fig. 6 The plots of Langmuir isotherm and Freundlich isotherm for equilibrium data of basic blue 41 (**a**), congo red (**b**), phenol (**c**), Cr(VI) (**d**), and Pb(II) (**e**)

The adsorption isotherm explains the adsorbate interact with the adsorbent and the distribution of adsorbate molecules/ions between the liquid phase and solid phase by measuring the distribution coefficient. The Langmuir and Freundlich isotherm models were used to investigate the adsorption process. The five different adsorption isotherms by non-linear regression at 298 K, 308 K, and 318 K are illustrated in Fig. 6. And also, Table 3 gives the relevant parameters and normalized standard deviation. The applicability of the

Table 3 Isotherm parameters for the adsorbate onto OAC

Adsorbate	T (°C)	Langmuir				Freundlich		
		$q_{e.cal}$ (mg g^{-1})	K_L (L mg^{-1})	R^2	R_L	K_F (L mg^{-1})	n_F	R^2
BB-41	25	732.4	0.147	0.922	0.017	157.8	2.74	0.987
	35	763.2	0.171	0.936	0.014	176.1	2.77	0.992
	45	790.3	0.200	0.923	0.012	189.8	2.71	0.982
CR	25	521.6	0.082	0.999	0.030	78.7	2.68	0.929
	35	533.4	0.092	0.997	0.026	86.2	2.74	0.937
	45	549.5	0.104	0.986	0.023	97.7	2.84	0.959
Phenol	25	121.3	0.017	0.855	0.124	12.1	2.63	0.984
	35	129.4	0.017	0.860	0.125	12.7	2.62	0.985
	45	139.4	0.017	0.874	0.128	13.3	2.59	0.988
Cr(VI)	25	98.6	0.041	0.855	0.057	15.6	3.08	0.990
	35	105.1	0.040	0.847	0.058	17.2	3.13	0.990
	45	114.2	0.039	0.851	0.060	18.6	3.14	0.987
Pb(II)	25	135.0	0.109	0.988	0.022	32.0	3.76	0.896
	35	140.6	0.136	0.975	0.018	35.8	3.89	0.903
	45	145.2	0.165	0.972	0.015	39.1	4.00	0.906

isotherm models to the experimental data of adsorption process was compared by judging the correlation (R^2).

The correlation coefficient R^2 of Langmuir for CR and Pb(II) are all higher than 0.97, which suggest that the adsorption isotherms of CR and Pb(II) onto OAC follow the Langmuir isotherm model. These results assume the monolayer adsorption on structurally and energetically homogenous active sites and predict the monolayer coverage at the outer surface of adsorbent. On the other hand, the R^2 of Freundlich models for BB-41, phenol, and Cr(VI) are much larger than that of Langmuir model, indicating that the equilibrium data are best fitted to the Freundlich isotherm model, which supposes the adsorption process onto the heterogeneous adsorption sites with the different affinities of binding sites onto the surface of OAC. All R_L values are found to be less than 1 and bigger than 0 in each case, indicating that these adsorption processes are favorable. In addition, in the case of OAC, its saturation adsorption capacities at 25 °C are 686.4, 486.6, 115.3, 107.7, and 135.0 mg g^{-1} for BB-41, CR, phenol, Cr(VI), and Pb(II), respectively. This suggests that the OAC demonstrates high efficiency to remove the various pollutions from aqueous solution.

3.2.4 Kinetic Studies

Figure 7 shows that the variation in the adsorption of adsorbates as a function of contact time. Figure 7a shows the effect of contact time on the adsorbed amount of BB-41 by OAC from solution with initial concentrations of 200.0 mg L^{-1} at 25 °C. The adsorption capacity increases sharply with contact time in the first 20 min and attains equilibrium within 60 min. At the initial stage, the fast adsorption may be due to the higher driving force and the availability of the uncovered surface area and the active sites on the adsorbent. With the time increasing, the uncovered surface area and the active sites diminish and the decrease in the driving force takes long time to reach the equilibrium. As for other adsorbates, the same effect is observed on varying the contact time though the time of equilibrium is not the same.

The pseudo-first-order and pseudo-second-order models were applied to test adsorption kinetics data and further investigate the mechanism of adsorption. Kinetic parameters obtained from the pseudo-first-order and pseudo-second-order equations are listed in Table 4. The pseudo-second-order model fitted well with all experimental data (BB-41: $R^2 = 0.985$, CR: $R^2 = 0.995$, phenol: $R^2 = 0.994$, Cr(VI): $R^2 =$
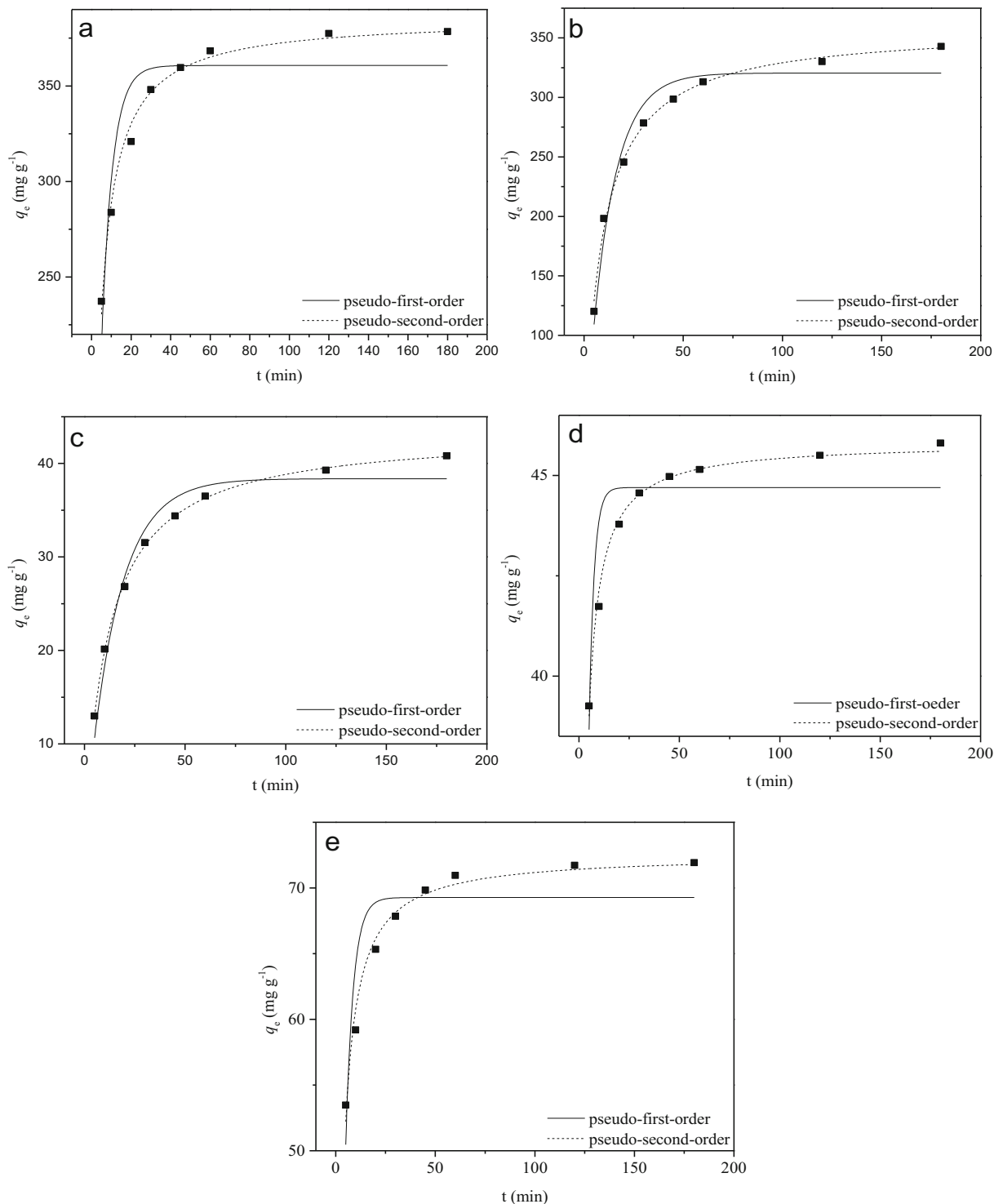
Fig. 7 The plots of pseudo-first-order and pseudo-second-order model for the kinetic data of basic blue 41 (**a**), congo red (**b**), phenol (**c**), Cr(VI) (**d**), and Pb(II) (**e**)

0.991, Pb(II): $R^2 = 0.980$). Moreover, the calculated $Q_{e(cal)}$ values agree very well with the experimental

data. It means that the adsorption rate is mainly determined by the chemical adsorption process.

Table 4 Comparison of the pseudo-first-order and pseudo-second-order kinetic parameter for the adsorption of BB-41, CR, phenol, Cr(VI), and Pb(II)

Adsorbate		Pseudo-first-order kinetics			Pseudo-second-order kinetics		
	$Q_{e\,(exp)}$ (mg g^{-1})	k_1 (min^{-1})	$Q_{e\,(cal)}$ (mg g^{-1})	R^2	k_2 (g mg^{-1} min^{-1})	$Q_{e\,(cal)}$ (mg g^{-1})	R^2
BB-41	378.5	0.180	360.7	0.837	0.0007	385.6	0.989
CR	342.8	0.079	320.5	0.950	0.0003	358.5	0.995
Phenol	40.8	0.065	38.4	0.959	0.0019	43.4	0.999
Cr(VI)	45.8	0.401	44.7	0.739	0.0250	45.8	0.991
Pb(II)	71.9	0.261	69.3	0.760	0.0071	72.5	0.980

3.2.5 Adsorption Thermodynamics

In order to investigate whether the adsorption is spontaneous and explore the mechanism involved in the adsorption process, the thermodynamic parameters were determined by the following equations:

$$\Delta G = -RT\ln K_d \qquad (8)$$

$$\ln K_d = \frac{\Delta S}{R} - \frac{\Delta H}{RT} \qquad (9)$$

where ΔS (J mol^{-1} K^{-1}), ΔH (kJ mol^{-1}), and ΔG (kJ mol^{-1}) are the entropy change, enthalpy change, and the Gibbs free energy change, respectively. R (8.314 J mol^{-1} k^{-1}) stands for the gas constant, T (K) is the temperature. K_d (q_e/C_e) is the thermodynamic equilibrium constant. The thermodynamic parameters are shown in Table 5.

The negative values of ΔG and the decrease in the negative of ΔG with an increase in temperature confirm that the adsorption process is spontaneous and a better adsorption performance can be obtained at a higher temperature. Meanwhile, the positive ΔH illustrates the endothermic nature of the adsorption, which is also consistent with the effect of temperature. $\Delta S > 0$ suggests that the increase in randomness at the solid-solution interface and a good affinity between adsorbate and adsorbent.

3.2.6 Adsorption Mechanism

The adsorption capacities obtained in this study are compared with other adsorbent adsorption capacities of these adsorbates as shown in Table 6 (Afroze and Sen 2018; Simón et al. 2018). It is observed that the adsorption capacities of OAC are higher than those of some other adsorbents. It is implied that OAC has the potential to be a good adsorbent which can be attributed to the high surface area. It is well known that a higher surface area can provide the availability of more adsorption sites which can improve the adsorption capacity at a degree. Comparing the experimental adsorption data of OAC, the adsorbent shows the highest adsorption capacity toward BB-41. The phenomena may be attributed to the coherence between the molecular size of the organic pollutants and the adsorbents' pore size as well as electrostatic interactions between the pollutants and adsorbents.

For organic pollution adsorption, it mainly depends on the molecular size of the organic pollution (the molecular size of organic adsorbate decreases in the

Table 5 Thermodynamic parameters for adsorption of adsorbates

Adsorbate	T	ΔG	ΔH	ΔS
BB-41	25	−21.5	17.72	131.42
	35	−22.7		
	45	−24.1		
CR	25	−19.0	8.27	92.12
	35	−19.9		
	45	−20.9		
Phenol	25	−8.6	5.72	47.91
	35	−9.0		
	45	−9.5		
Cr(VI)	25	−6.9	5.79	42.48
	35	−7.3		
	45	−7.8		
Pb(II)	25	−10.9	4.73	52.72
	35	−11.5		
	45	−12.0		

**Table 6** Comparison of adsorption capacities of different adsorbents for adsorbates

Adsorbates	Adsorbents	Adsorption capacity (mg g^{-1})	Reference
BB-41	Nanoporous silica	345	(Zarezadeh-Mehrizi and Badiei 2014)
	Bacillus macerans	89.2	(Atar et al. 2010)
	Clay mineral	84	(Kooli et al. 2015)
	OAC	686.4	This work
CR	Pine cone	435	(Dawood et al. 2014)
	Multiwall carbon nanotube	165.2	(Kamil et al. 2016)
	Bentonite	158.7	(Bulut et al. 2008)
	OAC	486.6	This work
Phenol	Commercial activated carbon	49.72	(Ozkaya 2006)
	Graphene	28.26	(Li et al. 2012)
	Porous carbon	83.88	(Liu and Zhang 2011)
	OAC	115.3	This work
Cr(VI)	Copolymer hydrogel	74.7	(Jiang et al. 2015)
	Ficusnitida leaves	21.0	(Ali and Alrafai 2016)
	Mesoporous carbon nitride	48.3	(Chen et al. 2014)
	OAC	107.7	This work
Pb(II)	Imprinted polymer	38	(Liu et al. 2011)
	Eggshell	90.90	(Putra et al. 2014)
	Tea residue	64.	(Yang and Cui 2013)
	OAC	135.0	This work

order of CR > BB-41 > phenol). Molecules with a suitable size would be adsorbed more favorably because they have more contact sites with the OAC surface. The inhibited diffusion of the relatively large size organic adsorbate (CR) into the small channels of OAC while a relatively small molecule (phenol) could enter the channels but could not be trapped. In detail, basic groups favor phenol adsorption whereas acidic groups favor BB-41 adsorption. Without pH adjustment, the OAC are negatively charged due to the carboxylic acid. Obviously, BB-41 being cationic has a high affinity for the negatively charged surfaces. The adsorbate (BB-41) could be absorbed when it possesses a moderate size toward the channels of adsorbent (OAC). Thus, the amount of BB-41 adsorption onto OAC is higher than the other two.

In addition, it is a high impact that the surface functional groups on the adsorbent toward the organic pollution uptake. It is observed that the removal performance is obvious when the adsorbate possesses the positively charged. As for the negatively charged adsorbate, the performance of adsorption is slightly inferior. It is attributed to the oxygen-containing functional groups

on the OAC surface. It is expected that the interaction of the molecules of dyes and the activated carbon surface occurs between the delocalized π electrons of the oxygen-free Lewis basic sites and the free electrons of the dye molecule present in the aromatic rings and multiple bonds. The presence of oxygen-containing
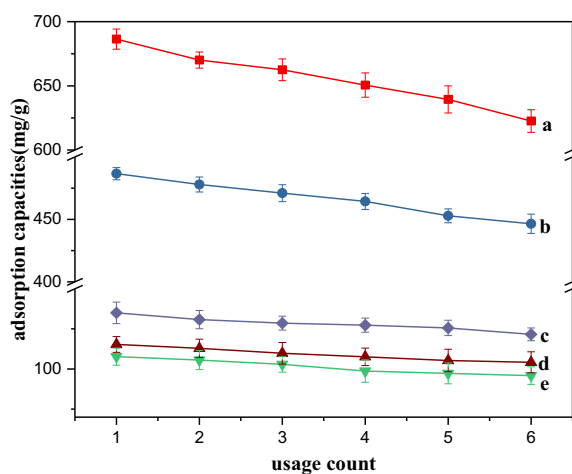
Fig. 8 Reusability of OAC for adsorption of basic blue 41 (**a**), congo red (**b**), Pb(II) (**c**), phenol (**d**), and Cr(VI) (**e**)
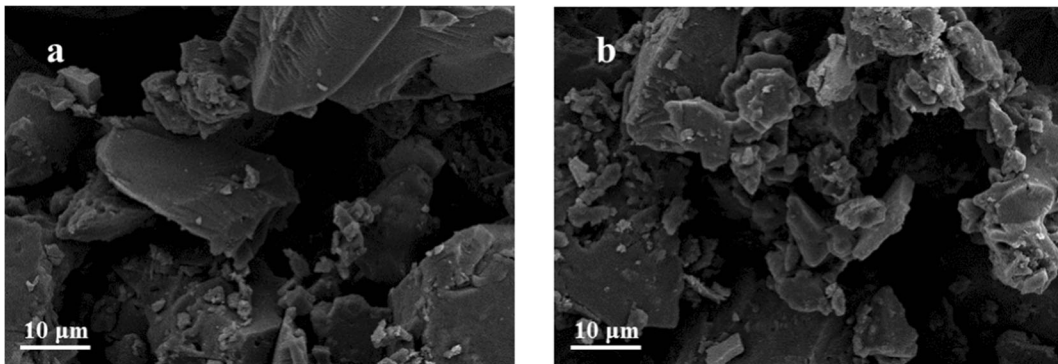
Fig. 9 SEM image of OAC before adsorption (**a**) and after four cycles (**b**)

functional group (an electron-withdrawing group) has a negative influence on the adsorption of an anionic species. These groups reduce the electron density of the OAC surface, thereby reducing the adsorption potential of the dye molecules.

The dominant adsorption interaction mechanism is electrostatic interactions between metal ions and OAC. OAC were materials with amphoteric character; thus, depending on the pH of the solution, their surfaces might be positively or negatively charged. At pH > pI, the carbon surface became negatively charged favoring the adsorption of cationic species. On the other hand, adsorption of anionic species will be favored at pH < pI. Cr(VI) and Pb(II) were selected as the anionic and cationic metal ion model. It is observed that the maximum removal efficiencies are obtained at 3.0 for Cr(VI) and 5.0 for Pb(II), respectively, which imply that the electrostatic interactions occur between the positively charged OAC and anionic metal ions at lower pH. At higher pH, the negatively charged is benefit for metal cationic ion adsorption by electrostatic interactions. Thus, it is concluded that OAC can be employed in removing various pollutants due to its universality.

3.3 Regeneration

The regeneration of the adsorbent was a key factor for improving wastewater process economics. Therefore, desorption experiments were also conducted. In order to display the reusability of the adsorbents, adsorption–desorption cycle of pollutants was repeated five times by using the same sorbent. The results were shown in Fig. 8, indicating that OAC could be used at least five times without significantly decrease in the adsorption capacity. Furthermore, a microscopic characterization of the

adsorbent after each cycle was conducted in order to check the structure stable of adsorbent. Adsorption–desorption cycle of BB-41 was repeated four times by using the same sorbent. The SEM images of OAC before adsorption and after four cycles are shown in Fig. 9. Obviously, after four cycles, the block structure of OAC was only slightly damaged. This phenomenon was also consistent with the results obtained from the regeneration experiment.

4 Conclusions

In summary, the agricultural by-product from peanut shell was converted to AC by $ZnCl_2$ activation at 500 °C and subsequently to OAC by concentrated nitric acid modification. The physicochemical characterization of OAC shows that it has a large specific surface area of 1807 m^2 g^{-1}. FT-IR spectrum of OAC indicated that the presence of some surface oxygen functional groups. The experimental maximum adsorption capacities of BB-41, CR, phenol, Cr(VI), and Pb(II) from aqueous solutions at 25 °C per 1 g of OAC are 686.4, 486.6, 115.3, 107.7, and 135.0 mg g^{-1}, respectively. This study indicates that OAC prepared from peanut shell and oxidized by nitric acid can be used as an effective adsorbent for the treatment wastewater containing various organic pollutants and heavy metal ions due to its universality adsorption performance.

Publisher's Note Springer Nature remains neutral with regard to jurisdictional claims in published maps and institutional affiliations.

References

Afroze, M., & Sen, T. K. (2018). A review on heavy metal ions and dye adsorption from water by agricultural solid waste adsorbents. *Water Air & Soil Pollution, 229*, 225.

Ahmad, R. (2009). Studies on adsorption of crystal violet dye from aqueous solution onto coniferous pinus bark powder (CPBP). *Journal of Hazardous Materials, 171*, 767–773.

Ahmadpour, A., & Do, D. (1996). The preparation of active carbons from coal by chemical and physical activation. *Carbon, 34*, 471–479.

Ali, I. H., & Alrafai, H. A. (2016). Kinetic, isotherm and thermodynamic studies on biosorption of chromium(VI) by using activated carbon from leaves of Ficus nitida. *Chemistry Central Journal, 10*, 1–19.

Atar, N., Olgun, A., & Çolak, F. (2010). Thermodynamic, equilibrium and kinetic study of the biosorption of basic blue 41 using bacillus maceran. *Engineering in Life Sciences, 8*, 499–506.

Babu, C. M., Binnemans, K., & Roosen, J. (2018). Ethylenediaminetriacetic acid-functionalized activated carbon for the adsorption of rare earths from aqueous solutions. *Industrial & Engineering Chemistry Research, 57*, 1487–1497.

Berber-Mendoza, M. S., Martínez-Costa, J. I., Leyva-Ramos, R., Garcia, H. J. A., & Castillo, N. A. M. (2018). Competitive adsorption of heavy metals from aqueous solution onto oxidized activated carbon fiber. *Water Air & Soil Pollution, 229*, 257.

Bhatnagar, A., Hogland, W., Marques, M., & Sillanpää, M. (2013). An overview of the modification methods of activated carbon for its water treatment applications. *Chemical Engineering Journal, 219*, 499–511.

Bo, Z., Fan, T., & Di, Z. (2008). Adsorption of copper ions from aqueous solution by citric acid modified soybean straw. *Journal of Hazardous Materials, 153*, 300–308.

Bonvin, F., Jost, L., Randin, L., Bonvin, E., & Kohn, T. (2015). Super-fine powdered activated carbon (SPAC) for efficient removal of micropollutants from wastewater treatment plant effluent. *Water Research, 90*, 90–99.

Boonamnuayvitaya, V., Sae-Ung, S., & Tanthapanichakoon, W. (2005). Preparation of activated carbons from coffee residue for the adsorption of formaldehyde. *Separation & Purification Technology, 42*, 159–168.

Bulut, E., Ozacar, M., & Sengil, I. A. (2008). Equilibrium and kinetic data and process design for adsorption of Congo red onto bentonite. *Journal of Hazardous Materials, 154*, 613–622.

Chen, H., Yan, T., & Jiang, F. (2014). Adsorption of cr(vi) from aqueous solution on mesoporous carbon nitride. *Journal of the Taiwan Institute of Chemical Engineers, 45*, 1842–1849.

Chen, H., Wang, X., Li, J., & Wang, X. (2015). Cotton derived carbonaceous aerogels for the efficient removal of organic pollutants and heavy metal ions. *Journal of Materials Chemistry A, 3*, 6073–6081.

Dawood, S., Sen, T. K., & Phan, C. (2014). Synthesis and characterisation of novel-activated carbon from waste biomass pine cone and its application in the removal of Congo red dye from aqueous solution by adsorption. *Water, Air, & Soil Pollution, 225*, 1818.

Ekrami, E., Dadashian, F., & Soleimani, M. (2014). Waste cotton fibers based activated carbon: Optimization of process and product characterization. *Fibers and Polymers, 15*, 1855–1864.

Gomez-Serrano, V., Cuerda-Correa, E. M., Fernandez-Gonzalez, M. C., Alexandre-Franco, M. F., & Macias-Garcia, A. (2005). Preparation of activated carbons from chestnut wood by phosphoric acid-chemical activation. Study of microporosity and fractal dimension. *Materials Letters, 59*, 846–853.

Guo, J., & Lua, A. C. (2003). Surface functional groups on oil-palm-Shell adsorbents prepared by HPO and KOH activation and their effects on adsorptive capacity. *Chemical Engineering Research & Design, 81*, 585–590.

Guo, R., Jiao, T., Li, R., Chen, Y., Guo, W., Zhang, L., Zhou, J., Zhang, Q., & Peng, Q. (2017). Sandwiched Fe3O4/carboxylate graphene oxide nanostructures constructed by layer-by-layer assembly for highly efficient and magnetically recyclable dye removal. *ACS Sustainable Chemistry & Engineering, 6*, 1279–1288.

Hesas, R. H., Arami-Niya, A., Wan, M. A. W. D., & Sahu, J. N. (2013). Preparation of granular activated carbon from oil palm shell by microwave-induced chemical activation: Optimisation using surface response methodology. *Chemical Engineering Research & Design, 91*, 2447–2456.

Jaramillo, J., Álvarez, P. M., & Gómez-Serrano, V. (2010). Preparation and ozone-surface modification of activated carbon. Thermal stability of oxygen surface groups. *Applied Surface Science, 256*, 5232–5236.

Jiang, Y., Li, F., Ding, G., Chen, Y., Liu, Y., Hong, Y., et al. (2015). Synthesis of a novel ionic liquid modified copolymer hydrogel and its rapid removal of cr (vi) from aqueous solution. *Journal of Colloid & Interface Science, 455*, 125–133.

Kamil, A. M., Mohammed, H. T., Alkaim, A. F., & Hussein, F. H. (2016). Adsorption of Congo red on multiwall carbon nanotubes: Effect of operational parameters. *Journal of Chemical & Pharmaceutical Sciences, 9*, 1128.

Kooli, F., Liu, Y., Al-Faze, R., & Suhaimi, A. A. (2015). Effect of acid activation of saudi local clay mineral on removal properties of basic blue 41 from an aqueous solution. *Applied Clay Science, 116-117*, 23–30.

Kumar, B., & Kumar, U. (2015). Adsorption of malachite green in aqueous solution onto sodium carbonate treated rice husk. *Korean Journal of Chemical Engineering, 32*, 1655–1666.

Li, Y., Du, Q., Liu, T., Sun, J., Jiao, Y., & Xia, Y. (2012). Equilibrium, kinetic and thermodynamic studies on the adsorption of phenol onto graphene. *Materials Research Bulletin, 47*, 1898–1904.

Li, Y., Du, Q., Liu, T., Peng, X., Wang, J., Sun, J., Wang, Y., Wu, S., Wang, Z., & Xia, Y. (2013). Comparative study of methylene blue dye adsorption onto activated carbon, graphene oxide, and carbon nanotubes. *Chemical Engineering Research and Design, 91*, 361–368.

Liu, Z., & Zhang, F. S. (2011). Removal of copper (ii) and phenol from aqueous solution using porous carbons derived from hydrothermal chars. *Desalination, 267*, 101–106.

Liu, Y., Liu, Z., Gao, J., Dai, J., Han, J., Wang, Y., et al. (2011). Selective adsorption behavior of pb(ii) by mesoporous silica sba-15-supported pb(ii)-imprinted polymer based on surface molecularly imprinting technique. *Journal of Hazardous Materials, 186*, 197–205.

Liu, Y., Meng, X., Luo, M., Meng, M., Ni, L., Qiu, J., Hu, Z., Liu, F., Zhong, G., & Liu, Z. (2014). Synthesis of hydrophilic surface ion-imprinted polymer based on graphene oxide for removal of strontium from aqueous solution. *Journal of Materials Chemistry A, 3*, 1287–1297.

Liu, Y., Zhong, G., Liu, Z., Meng, M., Liu, F., & Ni, L. (2016). Facile synthesis of novel photoresponsive mesoporous molecularly imprinted polymers for photo-regulated selective separation of bisphenol a. *Chemical Engineering Journal, 296*, 437–446.

Lo, S. F., Wang, S. Y., Tsai, M. J., & Lin, L. D. (2012). Adsorption capacity and removal efficiency of heavy metal ions by Moso and ma bamboo activated carbons. *Chemical Engineering Research & Design, 90*, 1397–1406.

Mirzaie, M., Rashidi, A., Tayebi, H. A., & Yazdanshenas, E. M. (2017). Removal of anionic dye from aqueous media by adsorption onto SBA-15/Polyamidoamine dendrimer hybrid: Adsorption equilibrium and kinetics. *Journal of Chemical and Engineering Data, 62*, 1365–1376.

Moussavi, G., & Khosravi, R. (2011). The removal of cationic dyes from aqueous solutions by adsorption onto pistachio hull waste. *Chemical Engineering Research & Design, 89*, 2182–2189.

Muniandy, L., Adam, F., Mohamed, A. R., & Ng, E. P. (2014). The synthesis and characterization of high purity mixed microporous/mesoporous activated carbon from rice husk using chemical activation with NaOH and KOH. *Microporous & Mesoporous Materials, 197*, 316–323.

Njoku, V. O., Islam, M. A., Asif, M., & Hameed, B. H. (2014). Utilization of sky fruit husk agricultural waste to produce high quality activated carbon for the herbicide bentazon adsorption. *Chemical Engineering Journal, 251*, 183–191.

Ozkaya, B. (2006). Adsorption and desorption of phenol on activated carbon and a comparison of isotherm models. *Journal of Hazardous Materials, 129*, 158–163.

Pezoti, O., Cazetta, A. L., Souza, I. P. A. F., Bedin, K. C., Martins, A. C., Silva, T. L., & Almeida, V. C. (2014). Adsorption studies of methylene blue onto ZnCl 2 -activated carbon produced from Buriti shells (Mauritia flexuosa L.). *Journal of Industrial & Engineering Chemistry, 20*, 4401–4407.

Piccini, G. M., Alessio, M., Sauer, J., Zhi, Y., Liu, Y., Kolvenbach, R., Jentys, A. & Lercher, J. A. (2015). Accurate adsorption thermodynamics of small alkanes in zeolites. Ab initio theory and experiment for H-Chabazite. Journal of Physical Chemistry C, 119.

Putra, W. P., Kamari, A., Yusoff, S. N. M., Ishak, C. F., Mohamed, A., Hashim, N., & Isa, I. M. (2014). Biosorption of cu (II), Pb (II) and Zn (II) ions from aqueous solutions using selected waste materials: Adsorption and characterisation studies. *Journal of Encapsulation and Adsorption Sciences, 4*, 25–35.

Ruiz-Fernández, M., Alexandre-Franco, M., Fernández-González, C., & Gómez-Serrano, V. (2011). Development of activated carbon from vine shoots by physical and chemical activation methods. Some insight into activation mechanisms. *Adsorption, 17*, 621–629.

Saleh, T. A., & Danmaliki, G. I. (2016). Influence of acidic and basic treatments of activated carbon derived from waste rubber tires on adsorptive desulfurization of thiophenes. *Journal of the Taiwan Institute of Chemical Engineers, 19*, 25–21.

Salman, J. M. (2014). Preparation of banana bunch fruits activated carbon for pesticides removal from aqueous solution.

Sekar, M., Sakthi, V., & Rengaraj, S. (2004). Kinetics and equilibrium adsorption study of lead(II) onto activated carbon prepared from coconut shell. *Journal of Colloid & Interface Science, 279*, 307–313.

Serkan Timur, I. C. K., Erdinc Ikizoglu, A., & Yanik, J. (2013). Preparation of activated carbons from Oreganum stalks by chemical activation. *Energy & Fuels, 20*, 2636–2641.

Shamsuddin, M. S., Yusoff, N. R. N., & Sulaiman, M. A. (2016). Synthesis and characterization of activated carbon produced from Kenaf Core Fiber using H_3PO_4 activation. *Procedia Chemistry, 19*, 558–565.

Shen, W., Li, Z., & Liu, Y. (2008). Surface chemical functional groups modification of porous carbon. *Recent Patents on Chemical Engineering, 1*, 27–40.

Simón, M., García, I., Diez-Ortiz, M., & González, V. (2018). Biochar from different carbonaceous waste materials: Ecotoxicity and effectiveness in the sorption of metal(loid)s. *Water Air & Soil Pollution, 229*, 224.

Van, T. H., Bui, T. T. P., & Nguyen, L. H. (2018). Residual organic compound removal from aqueous solution using commercial coconut Shell activated carbon modified by a mixture of seven metal salts. *Water Air & Soil Pollution, 229*, 292.

Wang, Z., & Chen, L. (2015). Adsorption characteristics of dibutyl phthalate from aqueous solution using ginkgo leaves-activated carbon by chemical activation with zinc chloride. *Desalination & Water Treatment, 54*, 1969–1980.

Yang, X., & Cui, X. (2013). Adsorption characteristics of pb (ii) on alkali treated tea residue. *Water Resources & Industry, 3*, 1–10.

Yu, Q., Li, M., Ning, P., Yi, H., & Tang, X. (2014). Preparation and phosphine adsorption of activated carbon prepared from walnut shells by KOH chemical activation. *Separation Science & Technology, 49*, 2366–2375.

Yue, Z., Mangun, C. L., & Economy, J. (2002). Preparation of fibrous porous materials by chemical activation: 1. ZnCl2 activation of polymer-coated fibers. *Carbon, 40*, 1181–1191.

Zarezadeh-Mehrizi, M., & Badiei, A. (2014). Highly efficient removal of basic blue 41 with nanoporous silica. *Water Resources & Industry, 5*, 49–57.